ACS APPLIED MATERIALS & INTERFACES

Research Article

www.acsami.org

Fabrication of Novel Two-Dimensional Nanopatterned Conductive PEDOT:PSS Films for Organic Optoelectronic Applications

Lucia Petti,*[,†] Massimo Rippa,[†] Rossella Capasso,[†] Giuseppe Nenna,[‡] Anna De Girolamo Del Mauro,[‡] Giuseppe Pandolfi,[‡] Maria Grazia Maglione,[‡] and Carla Minarini[‡]

[†]Cybernetics Institute of CNR, 80072 Pozzuoli, Italy

[‡]UTTP ENEA Portici Research Centre, 80055 Portici, Italy

Supporting Information

ABSTRACT: This paper presents a novel strategy to fabricate two-dimensional poly(3,4 ethylenedioxythiophene):poly(styrene sulfonate) (PEDOT:PSS) photonic crystals (PCs) combining electron beam lithography (EBL) and plasma etching (PE) processes. The surface morphology of PEDOT:PSS PCs after mild oxygen plasma treatment was investigated by scanning electron microscopy. The effects on light extraction are studied experimentally. Vertical extraction of light was found to be strongly dependent on the geometric parameters of the PCs. By changing the lattice type from triangular to square and the geometrical parameters of the photonic structures, the resonance peak could be tuned from a narrow blue emission at 445 nm up to a green emission at 525 nm with a full width at half-maximum of 20 nm, which is in good agreement with Bragg's diffraction theory and free photon band structure. Both finite-difference time-domain and plane wave expansion methods are used to calculate the resonant frequencies and the photonic band structures in the two-dimensional photonic crystals showing a very good agreement with the experiment results. A 2D nanopatterned transparent anode was also fabricated onto a flexible polyethylene terephthalate (PET) substrate and it was integrated into an organic light-emitting diode (OLED). The obtained results fully confirm the feasibility of the developed process of micro/nano patterning PEDOT:PSS. Engineered polymer electrodes prepared by this unique method are useful in a wide variety of high-performance flexible organic optoelectronics.

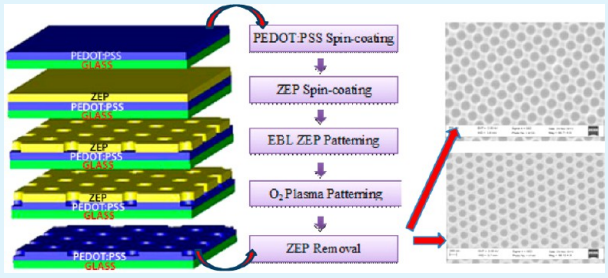

KEYWORDS: *photonic crystals, efficiency, light extraction, polymeric electrodes, flexible OLED*

INTRODUCTION

OLEDs and OPVCs will play a fundamental role in the new frontiers of the organic electronic (OE) devices because of the efficiency achievements, the ease in the realization processes, and the possibility of making the devices on flexible substrates. One of the essential points to ensure a future in the development of this technology is the device quantum efficiency that will give to this device classes a key role in the new frontier of lighting and energy storage.

It is widely known that the external quantum efficiency of conventional OLED devices remains near 20% because of losses due to wave-guiding effect. Recently, there has been great progress to enhance the light out-coupling efficiency of organic electroluminescent devices by means of various internal and external device modification techniques. Several strategies were developed concerning the surface modification to increase the efficiency factor by using ordered microlenses, bragg reflectors, 2D photonic crystals or modifying the cavity effects.[1−4] OLED and LED with a two-dimensional photonic crystal structure have been fabricated by several groups.[5−13] To fabricate a nanoscale pattern, e-beam lithography (EBL),[14] laser interference lithography (LIL),[15] self-assembled clusters (SACs),[16] and nanoimprint lithography (NIL)[8−12] have been used.

To simplify the device architecture of 2D-PC OLEDs, a first effort on partially structured ITO electrode was realized by Fujita et al.[17] who showed an improvement in efficiency due to the enhancement of light extraction for confined modes in ITO/organic layers by photonic crystal effect. More recently, an ITO electrode was partially patterned by focused ion beam (FIB) covered by PEDOT:PSS finding an increased efficiency.[18] However, ITO has problems of scarce indium on earth, high mechanical brittleness that makes it unsuitable for flexible electronic devices, and poor adhesion to organic and polymeric materials. Therefore, there is strong demand for new transparent conductive materials to replace ITO. Among them, PEDOT:PSS has gained strong attention. PEDOT:PSS is widely used as an anode buffer layer in both polymer light-emitting diodes[19,20] and OLEDs.[6,21,22] The reason why PEDOT:PSS is traditionally used as buffer layer instead of anode is because of its limited conductivity. There have been several works reported on the improvement of the conductivity, work function, and morphology of PEDOT:PSS layers,

Received: January 9, 2013
Accepted: May 2, 2013
Published: May 2, 2013

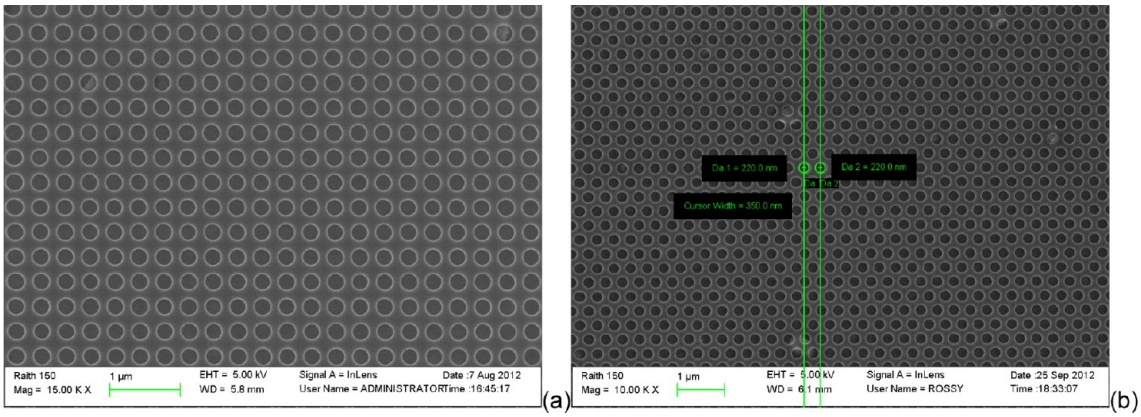

Figure 1. SEM images of the 2D PCs obtained arranging cylindrical air rods into the ZEP polymer matrix 200 nm thick after EBL direct writing; (a) square-lattice with rods of diameter D = 260 nm and lattice constant a = 350 nm; (b) triangular-lattice with rods of diameter D = 220 nm and lattice constant a = 350 nm.

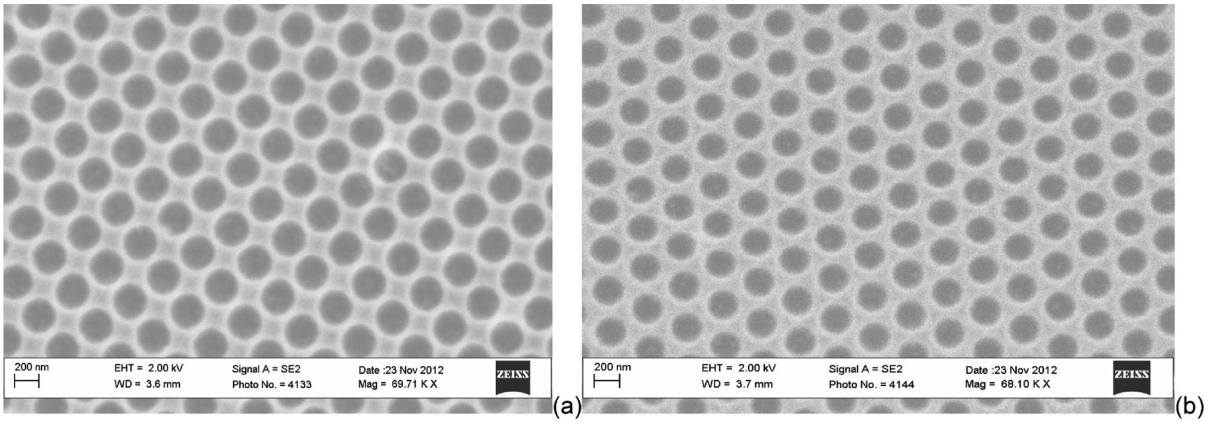

Figure 2. SEM images of the 2D PCs obtained after the PE process showing 100 nm thick cylindrical air rods into the PEDOT:PSS polymer matrix; (a) square lattice with rods of diameter D = 260 nm and lattice constant a = 350 nm; (b) triangular lattice with rods of diameter D = 220 nm and lattice constant a = 350 nm.

including mixture with organic solvents, and addition of dopants.[21−30] PEDOT:PSS electrodes with conductivities up to 3000 S/cm have been reported for polymer solar cells.[29] However, as many polymer materials, PEDOT:PSS is very difficult to be patterned, unlike traditional inorganic metal electrode materials, which can be easily engineered into various wanted micro/nanostructures. Thereby, it would be very meaningful if ways capable of engineering PEDOT:PSS film can be developed; this is even so considering that PEDOT:PSS is the only workable polymer electrode material at present. Very few studies have been reported on surface modification of PEDOT:PSS layers for OLED and organic solar cell applications but no reports on their processability in terms of direct nanopatterning are available. Previously reported PEDOT:PSS structures by nanoimprinting are limited to microscale structures with low aspect ratios (AR ∼ 10^{-2}).[31] Because of this patterning challenge, the application of imprinting PEDOT:PSS nanostructures for devices has been very limited. X. Zhou et al.[32] observed that mild oxygen plasma-treated PEDOT:PSS as anode buffer layer exhibited significantly enhanced lifetime and decreased driving voltage. U. Lemmer et al.[33] patterned PEDOT:PSS anodes with an oxygen plasma without destroying its outstanding electrical properties. Some simulation on 1D structured PEDOT:PSS was already reported and it was demonstrated that this 1D structure is beneficial for both optical and electrical properties and could improve the absorption of light by organic solar cells for wavelengths close to the band gap of the material.[34]

Here, to the best of our knowledge, we introduce for the first time an effective process based on the combination of EBL and PE techniques to fabricate a novel polymeric anode structure based on 2D nanopatterned conductive PEDOT:PSS layers. The proposed ITO-free electrode structure has been integrated into a flexible OLED device.

EXPERIMENTAL METHODS

Fabrication of 2D Patterned PEDOT:PSS Nanostructures. Our experimental structures were fabricated by using high-resolution electron beam lithography (EBL) technique as a first step. The EBL facility employed consisted of a Raith 150 system. Such system enables the writing of patterns of arbitrary geometries with a spatial resolution up to 10 nm. The samples were obtained by exposing a layer of styrene methyl acrylate based polymer (ZEP) deposited on a conductive PEDOT:PSS spin coated onto a corning glass substrate. The e-beam is locally focused on the sample to expose selected regions of material homogenously along the depth of the substrate according to the calculated desired pattern. Exposed areas were dissolved away leaving a two-dimensional square-based photonic crystal and a triangular PC structure made of air filled cylinders, located at the vertices of the square and of the triangular lattice, respectively, lying in the ZEP polymer matrix. The arrangement of the air cylinders is shown schematically in images a and b in Figure 1.

A 200-nm-thick layer of ZEP was spin coated on the top of the cleaned substrate. Subsequently, the 2D nanopatterning was defined using the Raith 150 system with current and area dosage of 23.6 pA at 10 KeV. The resist was developed in n-amyl acetate. To test our process on different wavelengths, we fabricated different reciprocal lattice vectors (G_0) and different filling fractions of the lattices (F), a 2D-PC pattern with triangular and square lattices.[35] For the triangular lattice, air cylinders with diameter D = 220 nm and period of a = 350 nm have been uniformly formed by EBL on a surface of about 1.5 × 1.5 mm^2. Instead, for the square pattern, cylinders with D = 260 nm and period of a = 350 nm have been performed.

The nanopatterned ZEP layer was subsequently used as a sort of lithographic mask during the anisotropic plasma etching process. The PEDOT:PSS (700 S/cm^2) was obtained by doping the PEDOT: PSS with dimethylsulfoxide (DMSO) as described in a previous paper.[36] It was partially etched, obtaining the PEDOT:PSS photonic crystals, by a high-vacuum plasma enhanced chemical vapor deposition (PECVD) multichamber system[33] realized by an ELETTRORAVA with these parameters: power 30W, 30 sccm for the O_2, and pressure of 0.4 Torr for a process of 80 s. As the final step, N-methyl-2-pyrrolidone (NMP) solvent was used as ZEP removal without damaging the underlying PEDOT:PSS film. Figure 2 a-b shows representative SEM images of the fabricated 2D square and triangular lattice PEDOT-PSS PC patterns of size 1.5 × 1.5 mm^2. The period (a) and diameter (D) of the cylindrical air rods were measured to be 350 and 260 nm for the square lattice, and a = 350 nm with D = 220 nm for the triangular lattice, respectively, from the SEM images. The thickness of the air rods is of 100 nm and the remaining unstructured PEDOT:PSS film is 100 nm thick.

The general schematic of a fabrication flow is shown in Figure 3.

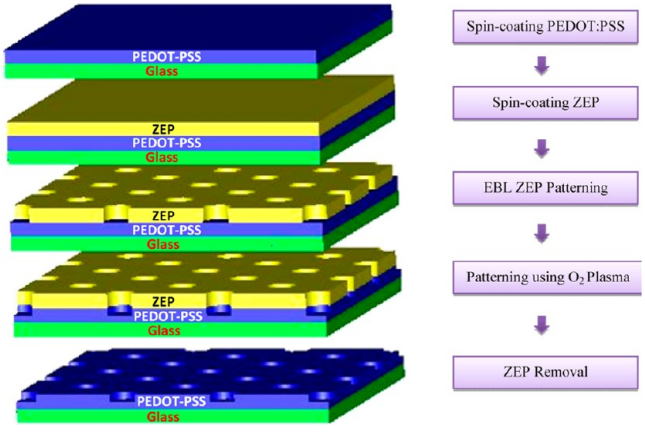

Figure 3. Schematic diagram/process for the conductive PEDOT:PSS-PC realization.

As a second step, we tested the method on a PET substrate so to confirm that our developed process works not only on glass but also on a flexible substrate. We patterned PEDOT:PSS nanostructures, forming 2D square-based PCs, with the same method described previously but using a PET substrate instead of a glass substrate. Air cylinders with D = 260 nm and period of a = 350 nm have been formed in a 200 nm thick ZEP layer by EBL on a PEDOT:PSS-coated (700 S/cm^2) PET as a first step. The nanopatterned ZEP layer acted as a lithographic mask during the anisotropic plasma etching process. As a second step, the PEDOT:PSS was partially etched by PECVD obtaining the 2D PEDOT:PSS photonic crystals. Finally, N-methyl-2-pyrrolidone (NMP) solvent was used as ZEP removal.

The light propagating in the glass substrate that is extracted by diffraction was measured at room temperature using the setup reported in Figure 4 comprising a white lamp used in Leica series microscopes, a multimode fiber, a CCD imaging telescope (OL610), and a spectroradiometer (OL770-LED).[37,38] This apparatus has been used to analyze the optical properties of our photonic crystals in order

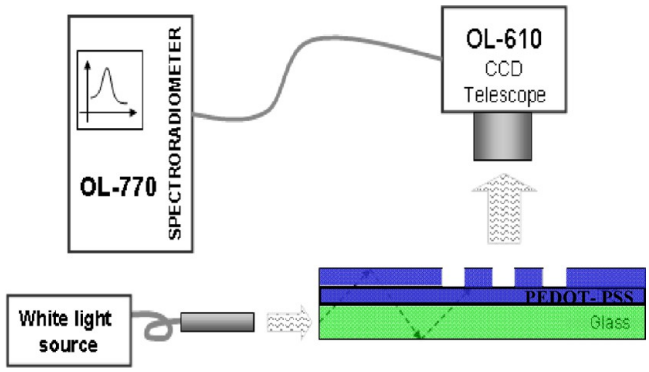

Figure 4. Optical set up employed for the PC spectra measurements.

to evaluate the resonances of the structures and the operational optical ranges.

Fabrication of Flexible OLED Based on 2D Nanopatterned PEDOT:PSS Anode. We progressed one step further and integrated the 2D PEDOT:PSS nanostructures into a real device such as an OLED. The OLED device under investigation was realized on PET (polyethylene terephthalate) and includes the following sequence of materials: doped DMSO PEDOT:PSS 200 nm/NPD (N,N′-di-1-naphthaleyl-N,N′-diphenyl-1,1′-biphenyl-4,4′-diamine) 35 nm/CBP ((4,4′-bis(N-carbazolyl)-1,1′-biphenyl): Ir(ppy)3 (6%) Tris[2-phenyl-pyridinato-C2,N] iridium(III)25 nm/BCP (bathocuproine) 10 nm/Alq3 (Tris-(8-hydroxyquinoline)aluminum) 10 nm/calcium 30 nm/aluminum 90 nm. The devices were fabricated on structured and unstructured PEDOT:PSS surface realized on the same substrate to prevent changes due to different growth conditions.

RESULTS AND DISCUSSION

In this work, we harness Bragg-diffraction effects to improve light extraction efficiency from the fabricated conductive PEDOT:PSS-PC structures. After the O_2 PE process and the subsequent ZEP removal, the PEDOT:PSS photonic crystal structures (see Figure 2) were tested introducing a white light from the edge of the glass substrate that propagated inside the glass itself due to the total internal reflection phenomena, as shown in Figure 4. The PC area was seen as blue (triangular) or green (square) because of the wavelength-selective diffraction by the hybrid PC.[8,12,17,38,39] The vertical extraction of the light, by the coupling of the modes guided by the PC slab to the free radiation via Bragg scattering, is ruled by a phasematching condition, namely by the conservation of the in-plane component of the momentum at the air−dielectric interface.[40]

To achieve the large enhancement of light extraction that is fundamental in application such as OLED devices, it is important to explore all the possible physical parameters that modify the light propagation via diffraction on nanometric patterns. As suggested from other works,[35] optimum PC lattice type depends on the inplane k-vector length β_i of the guided mode that should get diffracted and on the losses present in the OLED under study. In general, the larger the inplane k-vector length, the higher is the required number of reciprocal lattice vectors with the same length in order to diffract every in-plane direction of the guided mode. Maximized diffraction efficiency is achieved with a filling fraction of the lattices around $F \approx 0.45$.[35]

Here, to verify the validity of our method, we designed, simulated, realized, and characterized two different patterns, with different main reciprocal lattice vector and filling fraction. In particular, for the triangular lattice, the length of the main reciprocal lattice vector is $G_0 = (4\pi/3)^{1/2}a$ and the filling

dx.doi.org/10.1021/am401451r | ACS Appl. Mater. Interfaces 2013, 5, 4777−4782

fraction is 0.36, whereas for the square one, the main reciprocal lattice vector is $G_0 = a/2$ with a filling fraction of 0.43. Both structures have the pitch a = 350 nm. To this purpose, Figure 5

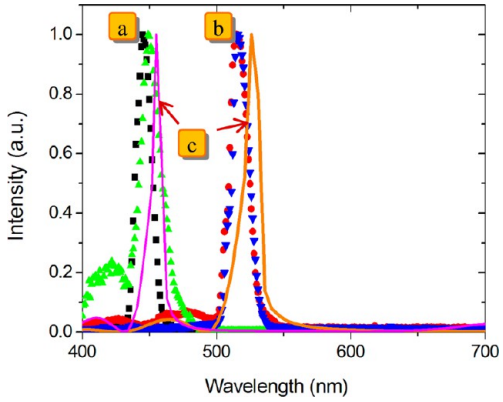

Figure 5. Measured and calculated emission spectra from the surface normal of the PCs: (a) triangular air-cylinders lattice with D = 220 nm and lattice constant a = 350 nm in ZEP matrix (black square dot curve) and in PEDOT:PSS matrix (green triangle dot curve), (b) square air-cylinders lattice with D = 260 nm and lattice constant a = 350 nm in ZEP matrix (red circle dot curve) and in PEDOT:PSS matrix (blue triangle dot curve), (c) simulated spectra of the triangular (magenta line) and square (orange line) PEDOT:PSS photonic crystals.

shows spectrally integrated light intensity characteristics of the triangular and square patterned samples as detected normally from the sample surface. The resonant peaks of the ZEP photonic crystals appear due to the PC feedback effect, and the full width at half-maximum of spectrum (fwhm) is of 20 nm at the main peaks that are located at λ = 445 nm and λ = 525 nm for the triangular lattice and for the square lattice, respectively. Vertical extraction of the light[35,38,40] found to be strongly dependent on the geometric parameters of the PCs structure, i.e., the order of the structure, the lattice constant, the dimensions of the cell elements.

For the PEDOT:PSS photonic crystals, we have a slight red shift of the spectra signals, probably due to the change in the crystals refractive index and/or minimum changes in the geometric quantities resulted from the realization steps (see Figure 3).

To verify our experimental findings, we have calculated the resonant frequencies of the structures. We employed a finite-difference time-domain numerical method (FDTD) performed with a commercial software (Full Wave simulation tool, RSoft Design Group, Ossining, NY). The time step (in units of ct) used is 66 × 10^{-4} mm. To simulate a periodic structure we use periodic boundary conditions on the $x-z$ plane, and perfectly matched layer boundary condition on y direction. The structures are excited from the air by a short impulse with a broad spectrum and plane wavefront. The simulated results are reported in Figure 5c. It is worthwhile to notice that the experimental resonances pretty well match the simulated peaks. From Figure 5, it is also possible to observe a further shift of the simulated signals compared to the experimental ones that can be easily explained as being due to the many approximations

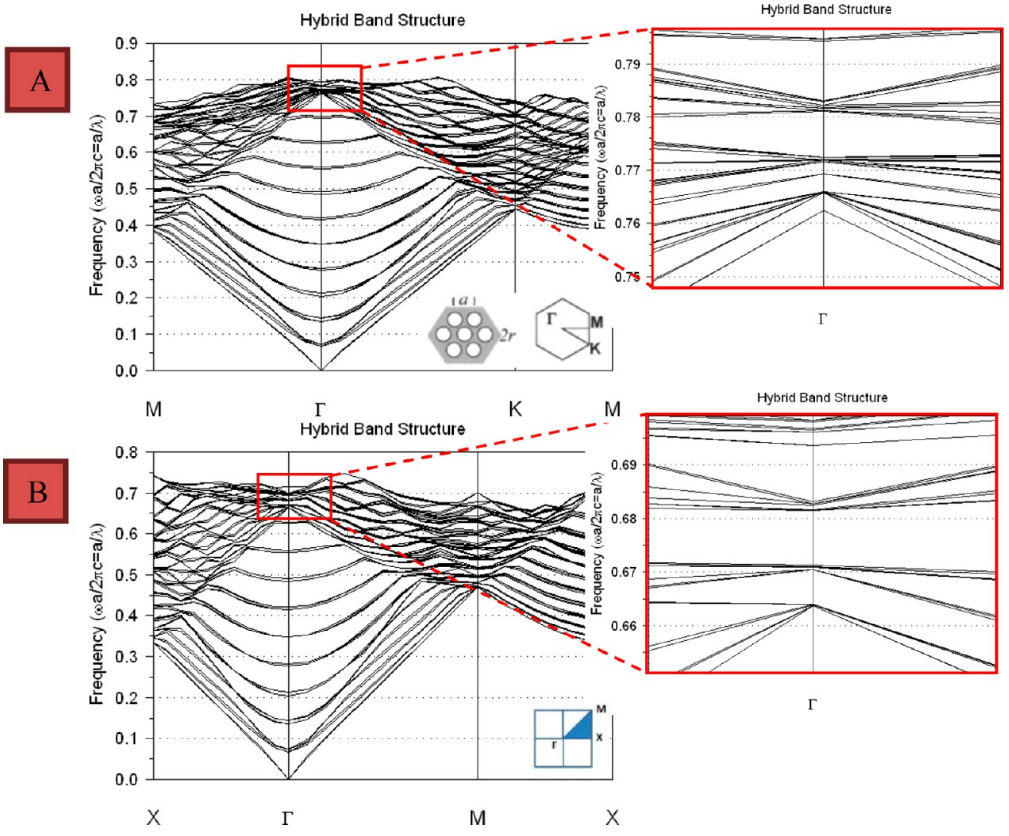

Figure 6. 3D PWE simulation results for the Pedot:Pss/glass PCs. Band diagram for Γ−M and Γ−X directions for (a) triangular lattice type (air hole radius r = 110 nm and period a = 350 nm); (b) square structures (air hole radius r = 130 nm and period a = 350 nm). The insets show the resonance at the Γ point corresponding to a band edge.

that need to be done in these cases. The dispersion relation of the different structures has been obtained using the plane wave expansion (PWE)[41] in a periodic medium consisting of infinitely long air cylinders in a dielectric material. The 3D simulation using a PWE method was performed with a simulation package (band SOLVE simulation tool, RSoft Design Group, Ossining, NY). For simplicity, we have assumed that the glass substrate (corning eagle 2000) and air are semi-infinite with a constant refractive index n_{glass}= 1.51 and n_{air} = 1, whereas the dispersion relation in the spectral region of interest has been used for the Pedot:Pss film. For the PEDOT:PSS/glass structure, the period was a = 350 nm, radius of the air holes r = 110 nm for triangular and r = 130 nm for the square structures, respectively, the thickness of the polymer t_{pedot} = 200 nm and depth of the holes t_{holes} = 100 nm. During the calculations we use a spatial grid with step size of 10 nm for the $x-z$ plane and 20 nm for the y direction. The numerical domain used corresponds to supercell of dimensions (1, 4, 1). In figure 6a we show the frequency density distribution of the first resonant band at Γ for the triangular crystal structure. The mode is singly degenerate with a frequency peak at the Γ point $\omega a/2\pi c$ = 0.78, as reported in Figure 6a. This value is in agreement with the experimental value of the main resonance peak λ = 445 nm reported in Figure 5. For the square crystal structure the experimental frequency peak is at λ = 525 nm (see Figure 5), and the simulated results show a resonant point at the Γ point $\omega a/2\pi c$ = 0.67 as reported in Figure 6b and its inset.

Considering an emission wavelength of 445 nm and of 525 nm, for the triangular lattice and for the square lattice, respectively, with a pitch of 350 nm (a/λ = 0.67 for square-type and 0.79 for triangular-type) for our samples, the pitch of 350 nm causes diffraction into the vicinity of the Γ-point and therefore a strong forward emission as $\theta_{air} = a \sin(\beta/k_0) \approx 0$ (with β being the propagation constant), and thus the resulting emission pattern is highly directional.[10−12]

In both cases, there are no band gaps and thus no band gap confinement, as expected. In our case, light propagated in a specific Γ−M direction or Γ−X direction for the triangular lattice and the square lattice, respectively, will be diffracted both in the opposite direction (−180°) and at angles of −90° and 90°. The resulting four equivalent light waves will be combined, causing a 2D resonator to form.[39]

The reported simulations demonstrate that the realized photonic structure was reproduced perfectly on the doped PEDOT:PSS film and that the developed process steps to engineer PEDOT:PSS film have been successfully achieved. We also want to underline that in a corrugated OLED the corrugation depth of the PC layers and the metal grating can be considered as identical and this might cause different optical effects that must be taken into account as previously mentioned.[42]

Current−voltage ($I-V$) and electroluminescence−voltage ($L-V$) characteristics of the fabricated flexible OLED devices based on the nanostructured polymeric anode are reported in Figure 7. They have been measured as described in a previous work.[37]

Figure 7 displays the current density−voltage ($J-V$) characteristics of the PC structured device. The turn-on voltage is approximately around 4 V. The inset shows the luminance behavior versus the device current density. From the graph, it is possible to have an idea of the efficacy improvement obtained by the structured device that can be evaluated to be a factor

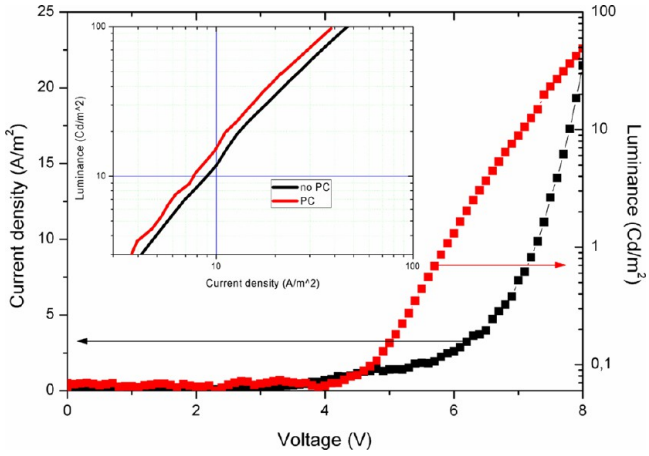

Figure 7. Current−voltage ($J-V$) characteristics of the PC structured device. In the inset we reported the luminance vs voltage ($L-V$) curves of both structured and unstructured devices.

around ∼1.25. It is a good result if we think that we realized the device structure entirely on a flexible substrate and in addition to a polymeric anode.[42]

The use of OLED and PC on extensible substrates[43,44] can give the opportunity to realize a new class of sensible devices revealing stress, strain or bending applied to the substrate and so to the PC structure. For this reason our study demonstrates the great potential of the developed combined process in realizing unconventional integrated OLED-PC structures that could be used not only in organic optoelectronic devices but also for sensing purposes.

CONCLUSIONS

In summary, we conclude that combining electron beam lithography and O_2 plasma etching is an effective way to pattern high-quality and high-density PEDOT:PSS photonic crystals. For the first time, to the best of our knowledge, 2D triangular and square photonic crystals have been fabricated directly on a conductive PEDOT:PSS film. The diffraction effect of our samples was confirmed, and consists of a narrow blue and green emission with a fwhm of 20 nm for the triangular and the square lattice, respectively. The measured resonances peaks due to the PC feedback effect have been compared with those theoretically calculated by both FDTD method and plane wave expansion method. There is good agreement between the experimental values and the numerical ones. The novel PEDOT:PSS photonic crystals increase the feasibility of using partially nanostructured PEDOT:PSS anodes to make extremely high-performance flexible organic optoelectronic devices by overcoming the major drawbacks of conventional ITO anodes. Finally, our method was tested on a flexible PET substrate and a 2D patterned PEDOT:PSS nanostructure has been integrated as a polymeric electrode surface in an OLED-PC device. This approach demonstrates a way to improve the device performance by replacing ITO anodes with flexible PEDOT-PSS anodes in a wide variety of organic optoelectronic devices.

ASSOCIATED CONTENT

Supporting Information

The manuscript was written through contributions of all authors. All authors have given approval to the final version of

the manuscript. This material is available free of charge via the Internet at http://pubs.acs.org.

AUTHOR INFORMATION

Corresponding Author

*E-mail: l.petti@cib.na.cnr.it.

Funding

This work has been financially supported by the Italian Ministry of Education, University and Research (MIUR) through the National Project entitled Relight (PN: PON02 00556 3306937).

Notes

The authors declare no competing financial interest.

REFERENCES

(1) Möller, S.; Forrest, S. R. *J. Appl. Phys.* **2002**, *91*, 3324−3327.
(2) Nenna, G.; De Girolamo Del Mauro, A.; Massera, E.; Bruno, A.; Fasolino, T.; Minarini, C. *J. Nanomater.* **2012**, *2012* (319398), 1−7.
(3) Lee, Y.-J.; Kim, S.-H.; Huh, J.; Kim, G.-H.; Lee, Y.-H.; Cho, S.-H.; Kim, Y.-C.; Rag Do, Y. *Appl. Phys. Lett.* **2003**, *82*, 3779−3781.
(4) Li, W.; Jones, R. A.; Allen, S. C.; Heikenfeld, J. C.; Steckl, A. J. *J. Display Technol.* **2006**, *2*, 143−152.
(5) Noda, S.; Fujita, M.; Asano, T. *Nat. Photonics* **2007**, *1* (8), 449−458.
(6) Koh, T.-W.; Choi, J.-M.; Lee, S.; Yoo, S. *Adv. Mater.* **2010**, *21*, 1−5.
(7) Boroditsky, M.; Krauss, T. F.; Coccioli, R.; Vrijen, R.; Bhat, R.; Yablonovitch, E. *Appl. Phys. Lett.* **1999**, *75*, 1036−1038.
(8) Ishihara, K.; Fujita, M.; Matsubara, I.; Asano, T.; Noda, S.; Ohata, H.; Hirasawa, A.; Nakada, H.; Shimoji, N. *Appl. Phys. Lett.* **2007**, *90*, 111114−111116.
(9) Rangel, E.; Matioli, E.; Chen, H.-T.; Choi, Y.-S.; Weisbuch, C.; Speck, J. S.; Hu, E. L. *Appl. Phys. Lett.* **2011**, *98*, 081104−081104.
(10) Lai, C.-F.; Kuo, H.-C.; Yu, P.; Lu, T.-C.; Chao, C.-H.; Yen, H.-H.; Yeh, W.-Y. *Appl. Phys. Lett.* **2010**, *97*, 013108−013110.
(11) Lai, C.-F.; Chao, C.-H.; Kuo, H.-C.; Yen, H.-H.; Lee, C.-E.; Yeh, W.-Y. *Appl. Phys. Lett.* **2009**, *94*, 123106−123108.
(12) Fujita, M.; Ishihara, K.; Ueno, T.; Asano, T.; Noda, S.; Ohata, H.; Tsuji, T.; Nakada, H.; Shimoji, N. *Jpn. J. Appl. Phys.* **2005**, *44*, 3669−3677.
(13) Cho, H. H.; Park, B.; Kim, H. J.; Jeon, S.; Jeong, J. H.; Kim, J. J. *Appl. Opt.* **2010**, *21*, 4024−4028.
(14) Lai, C.-F.; Kuo, H.-C.; Chao, C.-H.; Hsueh, H. T.; Wang, J. F. T.; Yeh, W-Y; Chi, J. Y. *Appl. Phys. Lett.* **2007**, *12*, 1231171−1231173.
(15) Divliansky, I. B.; Shishido, A.; Khoo, I. C.; Mayer, T. S.; Pena, D.; Nishimura, S.; Keating, C. D.; Mallouk, T. E. *Appl. Phys. Lett.* **2001**, *21*, 3392−3394.
(16) Gao, H.; Yan, F.; Zhang, Y.; Li, J.; Zeng, Y.; Wang, G. *J. Appl. Phys.* **2008**, *103*, 0143141−0143145.
(17) Fujita, M.; Ueno, T.; Asano, T.; Noda, S.; Ohata, H.; Tsuji, T.; Nakada, H.; Shimoji, N. *Electron. Lett.* **2003**, *39*, 1750−1752.
(18) Tsai, C.; Liao, L.; Luo, Y.; Chao, P. C.; Chen, E.; Meng, H.; Chen, W.; Lin, S.; Lin, C. *Microelectron. Eng.* **2010**, *87*, 1331−1335.
(19) Carter, S. A.; Angelopoulos, M.; Karg, S.; Brock, P. J.; Scott, J. C. *Appl. Phys. Lett.* **1997**, *70*, 2067−2069.
(20) Cao, Y.; Yu, G.; Zhang, C.; Menon, R.; Heeger, A. J. *Synth. Met.* **1997**, *87*, 171−174.
(21) Kim, W. H.; Makinen, A. J.; Nikolov, N.; Shashidhar, R.; Kim, H.; Kafafi, Z. H. *Appl. Phys. Lett.* **2002**, *80*, 3844−3846.
(22) Zhang, F.; Petr, A.; Dunsch, L. *Appl. Phys. Lett.* **2003**, *82*, 4587−4589.
(23) Snaith, H. J.; Kenrick, H.; Chiesa, M.; Friend, R. H. *Polymer* **2005**, *46*, 2573−2578.
(24) Mantovani, N. A.; Rene, A. J. J.; Martijn, K. *Adv. Funct. Mater.* **2008**, *18*, 865−871.
(25) Kim, J. Y.; Jung, J. H.; Lee, D. E.; Joo. *Synth. Met.* **2002**, *126*, 311−316.
(26) Ahlswede, E.; Mühleisen, W.; bin MohWahi, M. W.; Hanisch, J.; Powalla, M. *Appl. Phys. Lett.* **2008**, *92*, 143307−143309.
(27) Zimmermann, B.; Glatthaar, M.; Niggemann, M.; Riede, M. K.; Hinsch, A.; Gombert, A. *Sol. Energy Mater. Sol. Cells* **2007**, *91*, 374−378.
(28) Xia, Y.; Sun, K.; Ouyang. *Energy Environ. Sci.* **2012**, *5*, 5325−5332.
(29) Xia, Y.; Sun, K.; Ouyang. *Adv. Mater.* **2012**, *24*, 2436−2440.
(30) Choi, D. Y.; Kang, H. W.; Sung, H. J.; Kim, S. S. *Nanoscale* **2013**, *5*, 977−983.
(31) Emah, J. B.; Curry, R. J.; Silva, S. R. P. *Appl. Phys. Lett.* **2008**, *93*, 103301−103303.
(32) Zhou, Y.; Yuan, Y.; Lian, J.; Zhang, J.; Pang, H.; Cao, L.; Zhou, X. *Chem. Phys. Lett.* **2006**, *427*, 394−398.
(33) Colsmann, A.; Stenzel, F.; Balthasar, G.; Do, H.; Lemmer, U. *Thin Solid Films* **2009**, *517*, 1750−1752.
(34) Duche, D.; Simon, J. J.; Escoubas, L.; Torchio, P.; Le Rouzo, J.; Vervisch, W.; Flory, F. Photonic Crystals for Light Trapping within Organic Solar Cells. In *ICTON Mediterranean Winter Conference*; IEEE: Piscataway, NJ, 2009; pp 1−4; DOI: 10.1109/ICTONMW.2009.5385643 (accessed Dec 20, 2009).
(35) Wiesmann, C.; Bergenek, K.; Linder, N.; Schwarz, U. T. *Laser Photon. Rev.* **2009**, *3*, 262−286.
(36) De Girolamo Del Mauro, A.; Nenna, G.; Villani, F.; Minarini, C. *Thin Solid Films* **2012**, *520* (16), 5386−5391.
(37) Petti, L.; Rippa, M.; Capasso, R.; Nenna, G.; De Girolamo Del Mauro, A.; La Ferrara, V.; Pacheri Madathil, A.; Minarini, C. *J. Eur. Opt. Soc. Rapid Publ.* **2013**, *8*, 13002 1−13002 5.
(38) Petti, L.; Rippa, M.; Zhou, J.; Manna, L.; Mormile, P. *Nanotechnology* **2011**, *22*, 285307.
(39) Noda, S. *J. Lightwave Technol.* **2006**, *24*, 4554−4567.
(40) Fan, S.; Villeneuve, P. R.; Joannopoulos, J. D.; Schubert, E. F. *Phys. Rev. Lett.* **1997**, *78*, 3294−3297.
(41) Sakoda, K. In *Optical Properties of Photonic Crystals*; Rhodes, W. T., Asakura, T., Brenner, K.-H., Hansch, T. W., Krausz, F., Weber, H., Eds.; Springer: Berlin, 2005; p 56.
(42) Altun, A. O.; Jeon, S.; Shim, J.; Jeong, J.-H.; Choi, D.-G.; Kim, K.-D.; Choi, J.-H.; Lee, S.-W.; Lee, E.-S.; Park, H.-D.; Youn, J. R.; Kim, J.-J.; Lee, Y.-H.; Kang, J.-W. *Org. Electron.* **2010**, *11*, 711−716.
(43) Yu, Z.; Niu, X.; Liu, Z.; Pei, Q. *Adv. Mater.* **2011**, *23*, 3989−3994.
(44) Han, T.-H.; Lee, Y.; Choi, M.-R.; Woo, S.-H.; Bae, S.-H.; Hong, B. H.; Ahn, J.-H.; Lee, T.-W. *Nat. Photon.* **2012**, *6*, 483−487.